Published in final edited form as:
Magn Reson Med. 2010 June ; 63(6): 1493–1501. doi:10.1002/mrm.22347.

Triple Repetition Time Saturation Transfer (*TRiST*) ^{31}P Spectroscopy for Measuring Human Creatine Kinase Reaction Kinetics

Michael Schär[1,2], **AbdEl-Monem M. El-Sharkawy**[1], **Robert G. Weiss**[1,3], and **Paul A. Bottomley**[1]

[1] Russell H. Morgan Department of Radiology and Radiological Science, The Johns Hopkins University School of Medicine, Baltimore, MD, United States

[2] Philips Healthcare, Cleveland, OH, United States

[3] Cardiology Division, Department of Medicine, The Johns Hopkins University School of Medicine, Baltimore, MD

Abstract

Human cardiac phosphorus MR saturation transfer (ST) experiments to quantify creatine kinase (CK) forward rate constants (k_f) have previously been performed at 1.5T. Such experiments could benefit from increased signal-to-noise ratio and spectral resolution at 3T. At 1.5T, the four-angle ST method was applied with low-angle adiabatic pulses and surface coils. However, low-angle adiabatic pulses are potentially problematic above 1.5T due to bandwidth limitations, power requirements, power deposition and intra-pulse spin-spin decay. For localized metabolite spin-lattice relaxation time (T_1) measurements, a dual repetition time (2TR) approach with adiabatic half-passage pulses was recently introduced to solve these problems at 3T. Because the ST experiment requires a T_1 measurement performed while one reacting moiety is saturated, we adapt the 2TR approach to measure k_f using a Triple Repetition time ST (*TRiST*) method. A new pulsed saturation scheme with reduced sensitivity to static magnetic field inhomogeneity and compatibility with cardiac triggering is also presented. *TRiST* measurements of k_f are validated in human calf muscle against conventional ST, and found to agree within 3%. The first 3T *TRiST* measurements of CK k_f in the human calf (n=6), chest muscle and heart (n=8) are: 0.26±0.04s^{-1}, 0.23±0.03s^{-1} and 0.32±0.07s^{-1}, respectively, consistent with prior 1.5T values.

Keywords

saturation transfer; human heart; metabolism; reaction rate; high-energy phosphate; saturation pulses; creatine kinase and 3 Tesla

Introduction

Saturation transfer (ST) magnetic resonance spectroscopy (MRS) techniques enable the measurement of *in vivo* chemical reaction kinetics (1). The creatine kinase (CK) reaction has been studied in humans with phosphorus (^{31}P) ST MRS in the brain (2,3), skeletal muscle (4–8), and the heart (2,9). The CK reaction is the primary energy reserve of the heart. It

Corresponding author: Michael Schär, PhD, Johns Hopkins University School of Medicine, Department of Radiology; Park Bldg 326, 600 North Wolfe St., Baltimore, MD, 21287 USA, Tel. 410 502 4834, Fax 410 614 1977, michael.schar@gmail.com.

reversibly transfers high-energy phosphate between adenosine triphosphate (ATP) and phosphocreatine (PCr) through:

$$\mathrm{PCr+adenosinediphosphate+H^{+}} \underset{k_f}{\overset{k_r}{\leftrightarrow}} \mathrm{ATP+creatine}, \quad [1]$$

where k_f and k_r are the pseudo-first-order forward and reverse rate constants, respectively. In skeletal and heart muscle, the CK reaction putatively shuttles high-energy phosphate between the mitochondria, where ATP is created, and the myofibrils, where it is used. The four-angle saturation transfer (*FAST*) method enabled for the first time studies of CK kinetics in human heart at 1.5T (4), and to date remains the only localized ST method applied in patient studies (9–11). *FAST* demonstrated significant reductions in the forward ATP flux through CK in heart failure patients, even before a significant decline in ATP concentrations was observable (9,11). Because saturation transfer ^{31}P MRS might benefit significantly from an increased signal-to-noise ratio (SNR) and chemical shift dispersion at 3T, as compared to 1.5T (12–14), it is desirable to extend ST methods to human studies at 3T.

The effect of including chemical exchange in the Bloch Equations was first analyzed by Forsén and Hoffman (1). For the CK reaction, a two-site model of chemical exchange between PCr and the γ-phosphate resonance of ATP (γ-ATP) is typically assumed (reaction [1]). In the ST experiment the γ-ATP resonance is saturated by frequency-selective irradiation, reducing its magnetization to zero. As a result, the equilibrium longitudinal magnetization of PCr is reduced from $M_{0,PCr}$ to $M_{0,PCr}'$ and the spin-lattice relaxation time (T_1) of PCr is reduced from $T_{1,PCr}$ to an apparent $T_{1,PCr}'$, due to the chemical exchange of PCr with the saturated γ-ATP phosphate, where primes denote measurements performed in the presence of saturation. The longitudinal magnetization of PCr at time t while γ-ATP is saturated, $M_{PCr}'(t)$, is then given by:

$$M_{PCr}'(t)=M_{0,PCr}'+\left(M_{PCr}'(t=0)-M_{0,PCr}'\right)e^{\left(-\frac{t}{T_{1,PCr}'}\right)} \quad [2]$$

with $\frac{1}{T_{1,PCr}'}=\frac{1}{T_{1,PCr}^{intrinsic}}+k_f$ and $M_{0,PCr}'=\frac{M_{0,PCr}}{1+T_{1,PCr}^{intrinsic}k_f}$

where $T_{1,PCr}^{intrinsic}$ is the intrinsic longitudinal relaxation time, defined as the T_1 that would result in the absence of any exchange. The reaction rate is then given by:

$$k_f=\frac{1}{T_{1,PCr}'}\left(1-\frac{M_{0,PCr}'}{M_{0,PCr}}\right). \quad [3]$$

In practice, because the frequency selective saturation of γ-ATP may spillover into the PCr resonance, $M_{0,PCr}$ is typically measured with the same saturation applied at an equal spectral distance on the opposite side of the PCr resonance as a control (15–17). Thus, determination of k_f requires measurements of $T_{1,PCr}'$, $M_{0,PCr}'$, along with $M_{0,PCr}$ acquired with control saturation.

In the *FAST* method for measuring human CK kinetics at 1.5T (4,9–11), all of the variables, $T_{1,PCr}'$, $M_{0,PCr}'$ and $M_{0,PCr}$, are derived from partially-saturated measurements using the dual-angle method (18), applied twice in a total of four acquisitions. The availability of low-

angle adiabatic B_1-independent rotation (BIR-4) pulses (19) or BIR-4 phase-corrected (BIRP) pulses (20) to provide precise flip-angles over the sensitive volume of interest, is central to the success of this protocol when applied with the non-uniform radio frequency (RF) fields (B_1) afforded by surface coil excitation. However, the use of BIR4 or BIRP pulses with surface coil excitation is challenging at higher fields due to their high RF power requirements and the correspondingly high local RF power deposition near the coil (21). Increasing the pulse duration reduces the power, but limits the excitation bandwidth and can confound quantification with flip-angle dependent spin-spin relaxation (T_2) effects (21). Moreover, we recently showed that a dual repetition time (2TR) sequence using frequency-sweep cycled (FSC) adiabatic half-passage (AHP) 90° pulses, overcomes these problems, permitting accurate, efficient T_1 measurements at 3T (21). Because accurate T_1s are needed for calculating k_f, we now adapt this 2TR approach to the measurement of CK reaction rates in the human heart at 3T.

We present here a new method of performing ST ^{31}P MRS suitable for localized measurements of CK reaction kinetics at higher fields, wherein the variable BIR4/BIRP pulses are replaced by AHP pulses and variable repetition periods, TR, while retaining the scan-time efficiency of *FAST*. $T_{1,PCr}'$ and $M_{0,PCr}'$ are measured by the 2TR method with γ-ATP saturated, and $M_{0,PCr}$ is measured with a third, fully-relaxed AHP acquisition during control saturation. Thus, the total number of acquisitions reduces from the four in *FAST*, to three with this Triple Repetition time Saturation Transfer (*TRiST*) method. In addition, a pulsed saturation scheme is presented which is less sensitive to static magnetic field (B_0) inhomogeneities than the continuous irradiation used with *FAST* (4–8), and more amenable to cardiac triggering. The *TRiST* method is validated by comparison with conventional saturation transfer k_f measurements performed in human calf muscle. *TRiST* is combined with one-dimensional chemical shift imaging (1D CSI) to obtain the first 3T measures of CK kinetics in the human heart.

Methods

Calculating k_f from *TRiST*

In the *TRiST* experiment one measures the partially saturated magnetization $M_{z,PCr}'(TR_{short})$ and $M_{z,PCr}'(TR_{long})$ at short (TR_{short}) and long (TR_{long}) repetition periods in the presence of saturating irradiation applied to the exchanging CK moiety, γ-ATP at −2.5ppm, relative to PCr. Then $M_{0,PCr}$ is measured fully-relaxed in the presence of control irradiation applied at +2.5ppm. $T_{1,PCr}'$ is obtained from $M_{z,PCr}'(TR_{short})$ and $M_{z,PCr}'(TR_{long})$ according to the 2TR method (21). Because there is no closed form solution for T_1 measured by the 2TR method, $T_{1,PCr}'$ is determined from a look-up table for the ratio $R = M_{z,PCr}'(TR_{long})/M_{z,PCr}'(TR_{short})$ generated for each experiment where:

$$R(TR_{short}, TR_{long}, T_1) = \frac{1 - e^{-TR_{long}/T_1}}{1 - e^{-TR_{short}/T_1}}, \quad [4]$$

With the value of $T_{1,PCr}'$ in hand, the fully-relaxed $M_{0,PCr}'$ is just $M_{z,PCr}'(TR_{short})/(1\text{-}exp(-TR_{short}/T_{1,PCr}'))$. The rate constant k_f is then determined from Equation [3].

Error analysis and choice of TRs

Monte Carlo simulations were performed to estimate the effect of low ^{31}P SNR on k_f determinations. Gaussian noise with a standard deviation (SD) of $\sigma = 0.16 M_{0,PCr}$ per acquisition was added 2000 times to the three acquisitions, $M_{z,PCr}'(TR_{short})$, $M_{z,PCr}'(TR_{long})$, and $M_{0,PCr}$ in Equations [3] and [4]. The TR of the fully-relaxed $M_{0,PCr}$ measurement

($TR_{control}$) was varied from 12s to 25s. The chosen σ corresponds to a realistic PCr SNR of the heart of ~30 in a 1D CSI acquisition performed without saturation at TR=16s, with 16 phase-encoding steps, two averages and 1 cm spatial resolution. A full range of combinations of the number of averages (NA) and cardiac-gated TRs that resulted in a fixed total scan time of 38±0.2 minutes for the three acquisitions were evaluated. This was the same scan time as used for the four *FAST* experiments (9). NAs were chosen as multiples of 2 as required for the FSC AHP pulses (21).

The simulations were performed over the expected range of k_f from 0.1 to 0.4s^{-1} (9,11), assuming $T_{1,PCr}$=5.8s for the control measurement (21). $T_{1,PCr}'$ was determined from Equation 2 assuming $T_{1,PCr}^{intrinsic}$=7s for cardiac PCr, dependent of k_f. The mean (bias) and the standard deviation (scatter) of the difference between the simulated k_f, and the input k_f, for all 2000 determinations of k_f, at each of 185 combinations of TRs, and NAs were determined and expressed as a percentage of the input k_f.

Frequency selective saturation

Candidate schemes for frequency-selective saturation include: low power continuous RF (2,4–6); pulse trains of multiple hyperbolic secant pulses (3); and a Delays Alternating with Nutations for Tailored Excitation (*DANTE*) (7,8,22) pulse train of short hard pulses. Continuous low power irradiation produces a narrow suppression band at a single frequency. Dividing the irradiation into DANTE sub-pulses leads to aliased suppression bands at frequency intervals given by the inverse of the sub-pulse repetition time. To keep these aliased suppression bands away from the spectral peaks of interest (in this case PCr), the sub-pulse repetition time has to be chosen sufficiently short. However, saturating with a train of DANTE sub-pulses does enable the scanner to check for an electrocardiographic (ECG) R-wave (23) in between them for cardiac triggering (Figure 1). After applying the DANTE pulse train for a period given by the minimum TR minus the trigger delay and the acquisition time, the system checks for R-waves. Once an R-wave is detected, the pulse train continues for the trigger delay period.

The suppression band at the target frequency is rather narrow at low irradiation power for both the DANTE pulse train and for a continuous irradiation. This is desirable to minimize spillover irradiation onto the PCr resonance frequency. However, at 3T, B_0 inhomogeneity over the heart deteriorates due to the higher susceptibility as compared to 1.5T. This compromises the ability to saturate the γ-ATP resonance everywhere in the heart. To broaden the saturated frequency span, the amplitude of the DANTE pulse train is modulated according to the flip-angle function $\alpha(k)$:

$$\alpha(\mathrm{k})=\beta\sum_{\mathrm{n}=0}^{\mathrm{m}-1}\cos\left(2\pi(\mathrm{n}-\frac{\mathrm{m}-1}{2})\mathrm{k}\tau\delta\right), \quad [5]$$

to generate multiple adjacent suppression bands (24). Here k counts the sub-pulses, m is the number of suppression bands, δ is the frequency separation [Hz] between them, β is the average sub-pulse flip-angle per suppression band, and τ is the repetition time [s] of the sub-pulses. Figure 1 shows the resulting RF wave-form.

The frequency selectivity of the saturation irradiation was first tested with numerical calculations of the longitudinal magnetization based on the Bloch equations with no chemical exchange, normalized with $M_{0,PCr}$=1. Saturation was applied for 20s with m=1 or m=5, δ=9Hz, and τ=0.91ms. The following observed 3T relaxation times were used for γ-ATP and PCr respectively: T_1=3.1s and 5.8s, corresponding to human heart (21); and

T_2=78ms and 334ms based on calf muscle (25). The flip-angle β was increased until the normalized M_z of γ-ATP was below 0.05 for a bandwidth of at least 40Hz. Using the same irradiation settings, the M_z of PCr was determined 130Hz off-resonance from the center of the saturation band to estimate the strength of the spillover saturation during control irradiation. Spillover Q was quantified as the ratio between $M_{0,PCr}$ acquired with and without control saturation (4). The saturation pulse sequence has to saturate γ-ATP magnetization at a distance of up to ~9cm from the coil. At areas close to the coil, the B_1 field gradient of the transmit coil is such that the transmit B_1 field strength is about 6 times larger than the saturation threshold at 9cm (21). As a consequence, Q increases monotonically with depth from the coil. Therefore, Q was also calculated at flip-angles 6 times larger than the β determined above.

Human studies

Human studies were approved by the Institutional Review Board at Johns Hopkins University and all participants provided written informed consent. The *TRiST* sequence was implemented on a 3T *Achieva* whole body scanner (Philips Healthcare, Best, The Netherlands) with broadband capabilities. The amplitude modulated DANTE saturation scheme as described above with m=5 and β=0.9° was implemented with hard sub-pulses of 100μs duration. After the saturation train, magnetization was excited with a 5ms FSC tan/tanh-modulated adiabatic half passage pulse (21), and 512 data samples acquired with a bandwidth of 3000Hz. As soon as the acquisition was finished, the DANTE saturation was restarted. A custom-made dual transmit and receive ^{31}P surface coil set with a calibrated transmit RF field of 25μT at 9cm depth (21) was used for all ^{31}P MRS acquisitions which were performed within FDA guidelines for specific absorption rate (SAR).

Saturation transfer measurements are reported for the calf muscle of six (age = 40±9 years, 2 women) and the hearts of eight (age = 30±9 years, 4 women) healthy volunteers. In all studies optimal coil position was confirmed by proton MRI prior to performing *TRiST*. This was followed by localized second-order shimming based on acquired B_0-maps (26). A non-localized ^{31}P spectrum was then acquired to center the RF transmit frequency between the PCr and the γ-ATP resonances, and to determine the saturation frequency at the γ-ATP resonance, followed by the *TRiST* protocol.

Leg studies

Non-localized (NL) acquisitions for comparing *TRiST* with conventional ST measurements were performed with and without control saturation using a TR of 25s (NA = 4; dummies, DU = 2 to establish a steady-state) and with γ-ATP saturation using a set of seven TR values of 0.75s (NA=30; DU=22), 1.5s (NA=8; DU=10), 2.5s (NA=4; DU=6), 4s (NA=2; DU=4), 6s (NA=2; DU=4), 10s (NA=2; DU=2), and 16s (NA=2; DU=2) to enable determination of $T_{1,PCr}'$ by conventional partial saturation (PS). Additionally 1D CSI with sixteen 1-cm thick slices was performed with and without control saturation at TR=25s (NA=2, DU=2) and with γ-ATP saturation at TRs of 1.5s (NA=8, DU=10) and 10s (NA=2, DU=2). Scan time duration prohibited acquisition of additional ^{31}P 1D CSI data sets with different TR values for comparing localized *TRiST* measures with localized conventional saturation transfer k_f values. The initial acquisitions recorded without saturation were used for centering the saturation frequency on the γ-ATP resonance, and for determining Q.

Heart studies

For cardiac studies axial cine images were acquired during free breathing to determine the trigger delay for acquisition at end-systole. Cardiac-triggered 1D CSI was performed with sixteen phase encodes over a 16cm field of view (nominal slice thickness of 1cm) on volunteers oriented prone with the heart above the ^{31}P coil set. As above, a first data set was

acquired without saturation to center the saturation frequency on the γ-ATP resonance in a slice with signal from the heart, and to provide an unsaturated control spectrum for measuring Q and for potentially measuring metabolite concentrations (9). Next, the 3 *TRiST* data sets were recorded with control saturation at $TR_{control} \geq 16$s (NA=2; DU=2), and with γ-ATP saturation at a TR corresponding to 2 heart beats (TR_{short}; NA=18; DU=12), and another of at least 10s (TR_{long}; NA=8; DU=2). The average TR of each triggered data set is determined from the scanner's physiology log files.

Data analysis

Data from the same 1D CSI slices from the same volunteer were processed identically. PCr signals were measured from peak heights after subtracting the baseline. The baseline was automatically determined as the line between the minima on either side of the PCr peak. The 7-point NL conventional PS saturation transfer data from calf muscle were fitted to a two-parameter curve,

$$M_{Z,PCr}(TR)=M_{0,PCr}{}'\left(1-e^{-TR/T_{1,PCr}{}'}\right) \quad [6]$$

to determine $T_{1,PCr}'$ and $M_{0,PCr}'$. $M_{0,PCr}$ is given by the TR=25s acquisition with control saturation. For *TRiST*, the values of $T_{1,PCr}'$ and $M_{0,PCr}'$ were determined with the 2TR method using the NL spectra acquired with TR=1.5s and 10s from the same data set. For the 1D CSI data, $T_{1,PCr}'$ and $M_{0,PCr}'$ were determined using the 2TR method and the two 1D CSI data sets with γ-ATP saturated, while $M_{0,PCr}$ was determined from the data set acquired with control saturation which was assumed to be fully-relaxed. k_f was calculated using Equation [3]. In each heart study, the results for 1D CSI slices covering the chest and the heart were averaged, while slices in between consisting of both chest and heart tissue as well as cases where $Q<0.5$ in the heart were discarded. All data are reported as mean ±SD. Paired t-testing was used to determine the significance of differences between conventional and *TRiST* measures of $T_{1,PCr}'$ and k_f in the same subjects. Non-paired t-testing was used to test the difference between the *TRiST* measures of k_f in the leg and the chest acquired in different subjects. A $p\geq 0.05$ was considered non-significant (ns).

Results

First, numerical calculations were performed to assess the utility of the modified DANTE pulse train for ST studies. The results are summarized in Table 1 and Figure 2. To achieve sufficient saturation ($M_{z,\gamma\text{-}ATP}<0.05$) over a band of 40Hz, an irradiation flip-angle β of 5.1° and 0.9° for the constant (m=1) and amplitude modulated (m=5) irradiation, respectively, are required. Amplitude modulated irradiation leads to reduced spillover (i.e. higher Q) both close to the coil (0.45 vs. 0.11) and at 9cm into the tissue (0.93 vs. 0.81), as compared to an unmodulated DANTE irradiation (Table 1). Figure 2 shows the calculated normalized longitudinal magnetization $M_{z,\gamma\text{-}ATP}$ after applying the DANTE frequency selective saturation for 20s. Figure 2a demonstrates the difference between a DANTE pulse train with constant amplitude (m=1) and with amplitude modulation (m=5) as used in the human studies and applied with the β=0.9° flip-angle. Figure 2b plots normalized computed $M_{z,\gamma\text{-}ATP}$ overlaid over a cardiac ^{31}P spectrum. Breaking up the saturation into sub-pulses with a repetition time τ=0.91ms leads to aliased saturation at 1100Hz, which lies outside of the spectral region of interest.

The results of the Monte Carlo simulations are exemplified in Figure 3 for TR_{short} =1.7s. They show that for cardiac acquisitions, TR_{short}=1.7s, NA=18; TR_{long}=10s, NA=8; and

$TR_{control}$=16s, NA=2, result in an average relative % SD in k_f over the range 0.1–0.4 s^{-1} of 13.4%, reflecting the SNR assumed for these simulations. This introduces an average bias error that underestimates k_f by only 4.1%. The results of Figure 3 are not appreciably affected by reducing TR_{short} to ~0.85s even though the particular combinations of TR and NA that minimize the relative error vary in order to conserve the fixed scan-time constraint. Thus, with TR_{short}=0.85s, for example corresponding to one cardiac period, NA doubles to 36; while TR_{long}=10s, NA=8; $TR_{control}$=16s and NA=2 are unchanged, resulting in essentially the same average relative % SD in k_f of 12.1% and bias of 4.1%.

For validation purposes, $T_{1,PCr}'$ was determined with both the 7 point PS and the 2TR methods in NL calf muscle experiments. Figure 4 plots the measured PCr peak heights of the seven acquisitions and the resulting mono-exponential $T_{1,PCr}'$ fits from one volunteer. On average over all volunteers, $T_{1,PCr}'$ was 2.37±0.21s with the NL 7 point PS method, and 2.29±0.22s with the NL 2TR method, a difference in means of only 3% (p=ns). The maximum difference in $T_{1,PCr}'$ for the two methods in a single volunteer was 6.1%. The acquisitions required to measure $T_{1,PCr}'$ using the 7 point PS method were recorded in a total of 253s, as compared to 67s for *TRiST* for a 73% savings in scan-time for this measurement. Mean k_f determined non-localized with PS and *TRiST* in calf muscle were the same at 0.25±0.04s^{-1} and 0.26±0.04s^{-1} (p=ns), respectively.

Next, *TRiST* was combined with 1D CSI in leg to test whether it yielded the same localized k_f values. Figure 5 shows a representative *TRiST* dataset acquired in the leg of the same volunteer as the data shown in Figure 4. Figure 6 plots k_f measured NL in the calf for all volunteers using both conventional PS ST and *TRiST*, along with localized 1D CSI results from the calf muscle using *TRiST*. The localized 1D CSI results in the calf muscle agree with the NL results demonstrating that this localization scheme does not adversely affect *TRiST* (Figure 6).

TRiST with 1D CSI localization was then applied to the torso to measure k_f in the human heart. Figure 7 shows a *TRiST* dataset from a 1D CSI localized slice in the heart of a volunteer. The localized *TRiST* 1D CSI k_f values from the chest and hearts of the 8 volunteers are included in Figure 6. In chest muscle *TRiST* yielded an average value of k_f=0.23±0.03s^{-1}in these volunteers, consistent with that of calf muscle (p=ns). In the heart k_f was 0.32±0.07s^{-1}, and $T_{1,PCr}'$ was 2.3±0.6s (n=8). By applying Equation [2] to each subject, this yields $T_{1,PCr}^{intrinsic}$=7 ± 2s, consistent with that used for the Monte Carlo analysis. *Q*, an index of the effect of spillover radiation on PCr, as measured in the same acquisitions is shown in Figure 8. In the calf, mean Q went from 0.5 close to the coil to around 0.9 at a depth of 9cm, consistent with the calculations (Table 1). Similarly, in the torso Q was 0.7 in the chest muscle and 0.9 deeper at the level of the heart. The total acquisition time for the *TRiST* experiments was 44±1 min, and the total exam time, including initial (re-)positioning of the volunteer, survey imaging and the no-saturation acquisition used to determine *Q* was 75±10 min. However, the no-saturation acquisition serves double-duty in providing the basis for quantifying metabolite concentrations, so that the forward CK flux, which is the product of k_f and [PCr], can be obtained from this same exam (9–11).

Discussion

We have presented a new saturation transfer method, *TRiST*, that can be combined with spatially-localized ^{31}P MRS for the efficient measurement of CK pseudo-first-order reaction rates *in vivo* at 3T. *TRiST* avoids problems associated with the power requirements, bandwidth and intra-pulse T_2 decay associated with variable flip-angle adiabatic pulses, by use of the AHP 90° pulses throughout, and varying TR instead. The *TRiST* k_f values of 0.23±0.03s^{-1} and 0.32±0.07s^{-1} obtained here for the first time at 3T for human chest and

heart muscle, respectively, agree well with prior published values of $0.22\pm0.07s^{-1}$ and $0.32\pm0.07s^{-1}$ acquired at 1.5T using the FAST method (9). Similarly, these first *TRiST* k_f values acquired in the human calf muscle at 3T are well within the published range for human skeletal muscle k_f using localized FAST and other unlocalized surface coil methods at lower field strengths (4–8).

In the present work, use of the 2TR method to measure $T_{1,PCr}'$ was validated against a standard partial saturation method with seven different TRs in the calf muscle. $T_{1,PCr}'$ measured with the two methods differed only 3% on average and 6% at most. Indeed, the 1D CSI localized k_f measures in the calf (Figure 6) show consistent, constant, k_f measures up to 9cm deep into the calf. This is despite the fact that the effect of the spillover saturation on PCr varies significantly over this range (Figure 8), as the hard DANTE sub-pulses cannot entirely compensate for the large variation in RF field provided by the surface transmit coil (Table 1). The measured spill-over *Q*-values (Figure 8) agree well with the numerically calculated ones in Table 1. Evidently, the use of control saturation for the measurement of $M_{0,PCr}$ provides more-or-less adequate correction for spillover for metabolites whose properties fall within the observed range for skeletal and heart muscle. A more stringent analysis of spillover irradiation as performed in (27) may further minimize spillover errors.

The Monte Carlo error analysis anticipated a lower error in k_f than the variation in k_f measured in volunteers, although the analysis did not include spillover effects. This may also reflect physiological variations in CK reaction kinetics among individuals. Note that the practical constraints imposed for the analysis: a constant total exam time; cardiac-gating; the 16 CSI phase-encoding steps; and the need to acquire a fully-relaxed control $M_{0,PCr}$, means that the options for optimizing the protocol to minimize errors in k_f are limited mainly to the TR_{short} acquisition. Even so, the Monte Carlo analysis suggests that little benefit to either the precision or the accuracy of k_f measurements is obtained for TR_{short} values varied between 0.85–1.7s, provided that NA is adjusted accordingly. Because most heart-rates can be accommodated within this range of TR_{short} simply by adjusting the gating interval to 1–3 cardiac periods, the *TRiST* experiment can be efficiently run by re-adjusting NA for the particular TR_{short} corresponding to the heart-rate, such that the total scan time remains about the same. Monte Carlo simulations performed with varying TRs to determine the effect of beat to beat variations on k_f within each acquisition, show that heart-rate variations of up to 15% (28) about the mean measured heart-rate, result in ≤0.6% errors in k_f for $0.1s^{-1}\leq k_f \leq 0.4s^{-1}$.

Both TRiST and FAST are also sensitive to flip-angle accuracy, as indeed are the T_1 measurements required by all ST methods: hence our use of adiabatic pulses. As shown previously (21), T_1 was accurate to within 5% out to depths of 9cm, which includes the anterior myocardium. In the present study we validated k_f measurements in the leg out to the same depth of 9cm. Even though the AHP pulses we used are constant above their threshold, we can compare the values of k_f that one would obtain if the effective flip-angle of the pulses were 85° or 95°, instead of the true 90° flip-angle assumed for the calculation. With the same parameters used in the Monte Carlo simulations, this 6% error in flip-angle results in just a 4% error in R, and a 7% error in both T_1' and k_f.

Recently Xiong et al. applied a three acquisition ST method to the open chest porcine heart and the intact rat brain at 4.7T yielding similar results for the CK reaction rate as those obtained by conventional techniques (29). They employed a scheme of pre-saturation delays that were numerically optimized for the expected k_f values, thereby permitting a reduction in TR_{long}, assuming immediate and complete γ-ATP suppression once the saturation is turned on. While the lower peak power of the DANTE pulse train in our protocol requires the entire inter-pulse interval to achieve complete saturation, it does maximize the time available for

saturated γ-ATP spins to exchange with PCr, while allowing for cardiac triggering between the pulses–all within SAR guidelines.

The two-site model for the CK reaction has long been assumed for ^{31}P ST MRS measurements of k_f, because the measured PCr peak only exchanges with γ-ATP. On the other hand, ATP also exchanges with inorganic phosphate (P_i) (30–32). Studying the three-site chemical exchange involving PCr and P_i, can require two-site selective irradiation, to measure reverse reaction rate constants, for example (33). Fortunately, the amplitude-modulated DANTE saturation can also be tailored for multi-site saturation for such studies, beyond the simple broadening of a single-site saturation described in the present study.

In conclusion, *TRiST* provides accurate measurements of *in vivo* muscle CK pseudo-first-order forward rate constants in the human leg that agree with conventional methods in the same exam, and CK rate-constants in the normal heart at 3T in scan times that are tolerable for human studies. The results are consistent with prior human studies using different methods and B_0 field strengths. The challenges of higher-field magnets for quantitative saturation transfer studies using surface coil spectroscopy appear soluble and human cardiac CK kinetics can now be quantified at 3T.

Acknowledgments

The authors would like to thank Ronald Ouwerkerk and Refaat Gabr for fruitful discussions and Tricia Steinberg for assistance with human studies.

Grant support

NIH: R01 HL56882, R01 HL61912 and a grant from the D.W. Reynolds Foundation

References

1. Forsen S, Hoffman RA. Study of Moderately Rapid Chemical Exchange Reactions by Means of Nuclear Magnetic Double Resonance. Journal of Chemical Physics. 1963; 39(11):2892.
2. Bottomley PA, Hardy CJ. Mapping Creatine-Kinase Reaction-Rates in Human Brain and Heart with 4-Tesla Saturation Transfer P-31 Nmr. Journal of Magnetic Resonance. 1992; 99(2):443–448.
3. Du F, Zhu XH, Qiao H, Zhang X, Chen W. Efficient in vivo 31P magnetization transfer approach for noninvasively determining multiple kinetic parameters and metabolic fluxes of ATP metabolism in the human brain. Magn Reson Med. 2007; 57(1):103–114. [PubMed: 17191226]
4. Bottomley PA, Ouwerkerk R, Lee RF, Weiss RG. Four-angle saturation transfer (FAST) method for measuring creatine kinase reaction rates in vivo. Magn Reson Med. 2002; 47(5):850–863. [PubMed: 11979563]
5. Horska A, Fishbein KW, Fleg JL, Spencer RG. The relationship between creatine kinase kinetics and exercise intensity in human forearm is unchanged by age. American journal of physiology. 2000; 279(2):E333–339. [PubMed: 10913033]
6. Rees D, Smith MB, Harley J, Radda GK. In vivo functioning of creatine phosphokinase in human forearm muscle, studied by 31P NMR saturation transfer. Magn Reson Med. 1989; 9(1):39–52. [PubMed: 2709995]
7. Goudemant JF, Francaux M, Mottet I, Demeure R, Sibomana M, Sturbois X. 31P NMR saturation transfer study of the creatine kinase reaction in human skeletal muscle at rest and during exercise. Magn Reson Med. 1997; 37(5):744–753. [PubMed: 9126949]
8. Wiedermann D, Schneider J, Fromme A, Thorwesten L, Moller HE. Creatine loading and resting skeletal muscle phosphocreatine flux: a saturation-transfer NMR study. Magma. 2001; 13(2):118–126. [PubMed: 11502426]
9. Weiss RG, Gerstenblith G, Bottomley PA. ATP flux through creatine kinase in the normal, stressed, and failing human heart. Proceedings of the National Academy of Sciences of the United States of America. 2005; 102(3):808–813. [PubMed: 15647364]

10. Bottomley PA, Wu KC, Gerstenblith G, Schulman SP, Steinberg A, Weiss RG. Reduced myocardial creatine kinase flux in human myocardial infarction: an in vivo phosphorus magnetic resonance spectroscopy study. Circulation. 2009; 119(14):1918–1924. [PubMed: 19332463]
11. Smith CS, Bottomley PA, Schulman SP, Gerstenblith G, Weiss RG. Altered creatine kinase adenosine triphosphate kinetics in failing hypertrophied human myocardium. Circulation. 2006; 114(11):1151–1158. [PubMed: 16952984]
12. Shivu GN, Abozguia K, Phan TT, Ahmed I, Henning A, Frenneaux M. (31)P magnetic resonance spectroscopy to measure in vivo cardiac energetics in normal myocardium and hypertrophic cardiomyopathy: Experiences at 3T. European journal of radiology. 2008 [Epub ahead of print].
13. Tyler DJ, Emmanuel Y, Cochlin LE, Hudsmith LE, Holloway CJ, Neubauer S, Clarke K, Robson MD. Reproducibility of (31)P cardiac magnetic resonance spectroscopy at 3 T. NMR in biomedicine. 2008; 22(4):405–413. [PubMed: 19023865]
14. Tyler DJ, Hudsmith LE, Clarke K, Neubauer S, Robson MD. A comparison of cardiac (31)P MRS at 1.5 and 3 T. NMR in biomedicine. 2008; 21(8):793–798. [PubMed: 18512846]
15. Baguet E, Roby C. Off-resonance irradiation effect in steady-state NMR saturation transfer. J Magn Reson. 1997; 128(2):149–160. [PubMed: 9356270]
16. Gadian DG, Radda GK, Brown TR, Chance EM, Dawson MJ, Wilkie DR. The activity of creatine kinase in frog skeletal muscle studied by saturation-transfer nuclear magnetic resonance. The Biochemical journal. 1981; 194(1):215–228. [PubMed: 6975619]
17. Horska A, Spencer GS. Correctly accounting for radiofrequency spillover in saturation transfer experiments: application to measurement of the creatine kinase reaction rate in human forearm muscle. Magma. 1997; 5(2):159–163. [PubMed: 9268080]
18. Bottomley PA, Ouwerkerk R. The Dual-Angle Method for Fast, Sensitive T-1 Measurement in-Vivo with Low-Angle Adiabatic Pulses. Journal of Magnetic Resonance Series B. 1994; 104(2): 159–167.
19. Garwood M, Ke Y. Symmetric pulses to induce arbitrary flip angles with compensation for RF inhomogeneity and resonance offsets. J Magn Reson Med. 1991; 94:511–525.
20. Bottomley PA, Ouwerkerk R. BIRP: an improved implementation of low-angle adiabatic (BIR-4) excitation pulses. J Magn Reson A. 1993; 103:242–244.
21. El-Sharkawy AM, Schär M, Ouwerkerk R, Weiss RG, Bottomley PA. Quantitative cardiac (31)P spectroscopy at 3 Tesla using adiabatic pulses. Magn Reson Med. 2009; 61(4):785–795. [PubMed: 19195018]
22. Bodenhausen G, Freeman R, Morris GA. Simple Pulse Sequence for Selective Excitation in Fourier-Transform Nmr. Journal of Magnetic Resonance. 1976; 23(1):171–175.
23. Fischer SE, Wickline SA, Lorenz CH. Novel real-time R-wave detection algorithm based on the vectorcardiogram for accurate gated magnetic resonance acquisitions. Magn Reson Med. 1999; 42(2):361–370. [PubMed: 10440961]
24. Eberhardt KW, Schär M, Barmet C, Tsao J, Boesiger P, Kozerke S. Linear response equilibrium. J Magn Reson. 2006; 178(1):142–154. [PubMed: 16226909]
25. Meyerspeer M, Krssak M, Moser E. Relaxation times of 31P-metabolites in human calf muscle at 3 T. Magn Reson Med. 2003; 49(4):620–625. [PubMed: 12652531]
26. Schär M, Kozerke S, Fischer SE, Boesiger P. Cardiac SSFP imaging at 3 Tesla. Magn Reson Med. 2004; 51(4):799–806. [PubMed: 15065254]
27. Gabr RE, Weiss RG, Bottomley PA. Correcting reaction rates measured by saturation-transfer magnetic resonance spectroscopy. J Magn Reson. 2008; 191(2):248–258. [PubMed: 18226939]
28. Task Force of the European Society of Cardiology and the North American Society of Pacing and Electrophysiology. Heart rate variability: standards of measurement, physiological interpretation and clinical use. Circulation. 1996; 93(5):1043–1065. [PubMed: 8598068]
29. Xiong Q, Li Q, Mansoor A, Jameel MN, Du F, Chen W, Zhang J. Novel strategy for measuring creatine kinase reaction rate in the in vivo heart. Am J Physiol Heart Circ Physiol. 2009; 297(3):H1010–1019. [PubMed: 19561307]
30. Lebon V, Dufour S, Petersen KF, Ren J, Jucker BM, Slezak LA, Cline GW, Rothman DL, Shulman GI. Effect of triiodothyronine on mitochondrial energy coupling in human skeletal muscle. The Journal of clinical investigation. 2001; 108(5):733–737. [PubMed: 11544279]

31. Lei H, Ugurbil K, Chen W. Measurement of unidirectional Pi to ATP flux in human visual cortex at 7 T by using in vivo 31P magnetic resonance spectroscopy. Proceedings of the National Academy of Sciences of the United States of America. 2003; 100(24):14409–14414. [PubMed: 14612566]

32. Schmid AI, Chmelik M, Szendroedi J, Krssak M, Brehm A, Moser E, Roden M. Quantitative ATP synthesis in human liver measured by localized 31P spectroscopy using the magnetization transfer experiment. NMR in biomedicine. 2008; 21(5):437–443. [PubMed: 17910026]

33. Ugurbil K, Petein M, Maidan R, Michurski S, From AH. Measurement of an individual rate constant in the presence of multiple exchanges: application to myocardial creatine kinase reaction. Biochemistry. 1986; 25(1):100–107. [PubMed: 3954984]

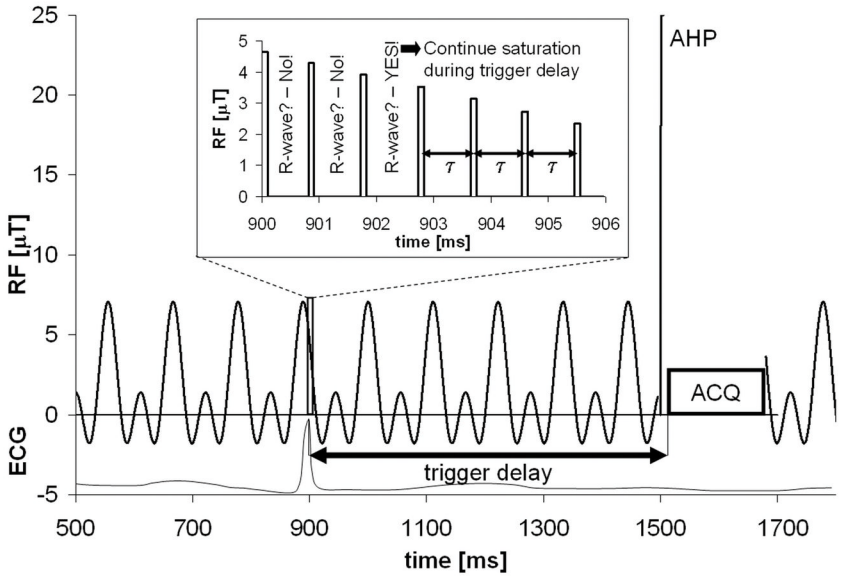

Figure 1.

Scheme of the *TRiST* acquisitions showing the amplitude modulation of the frequency selective RF saturation versus time. A zoomed version is shown in the inset where 100µs sub-pulses are used for real-time interrogation of the R-wave to enable cardiac triggering. The negative sign of the RF amplitude is to be understood as 180° phase shift. AHP and ACQ denote adiabatic half passage excitation and the acquisition window, respectively.

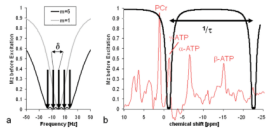

Figure 2.

Amplitude modulation of the DANTE pulse train as shown in Figure 1 broadens the saturated frequency span. (a) The calculated normalized longitudinal magnetization of γ-ATP after 20s of saturation around the saturation frequency with m=5 saturation bands δ=9Hz apart (black) as compared to a single band with m=1 (gray). (b) The saturation bands for m=5 DANTE saturation overlaid over the entire cardiac ^{31}P spectrum. The DANTE sub-pulse separation of τ=0.91ms leads to aliased saturation bands at $1/\tau$=1100Hz apart.

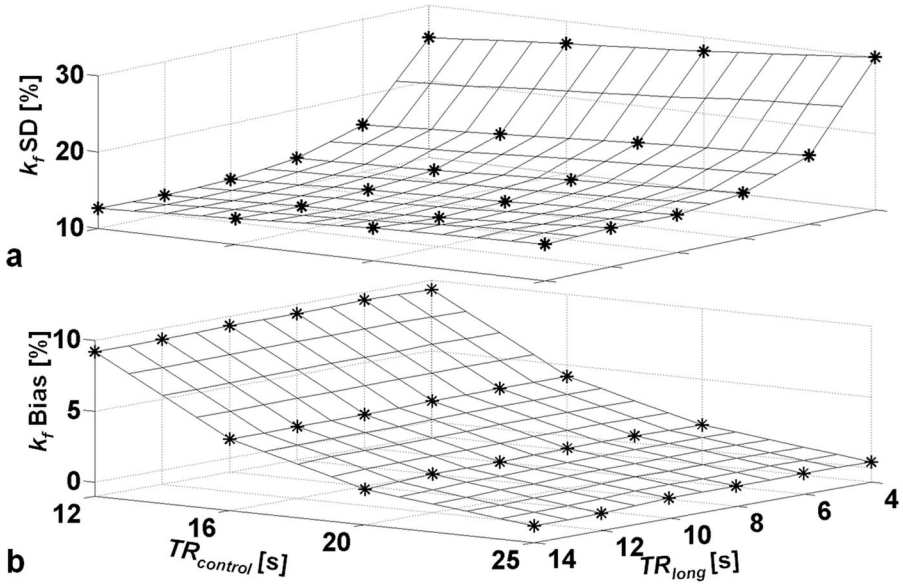

Figure 3.

Results from the Monte Carlo simulations of the *TRiST* experiment averaged over the k_f range 0.1 to 0.4s^{-1} as a function of TR_{long} (with γ-ATP saturated) and $TR_{control}$ (control saturation). TR_{short} was 1.7s (γ-ATP saturated) and NA combinations were chosen for a constant total study time of 38±0.2min. (a) The relative % SD in k_f for NA choices that lead to minimum error at each TR_{long} and $TR_{control}$ combination. (b) The average bias error in k_f, corresponding to the TR_{long}, $TR_{control}$ and NA combinations in part (a). A positive bias of 4% means that the observed k_f is less than the true k_f by 4%.

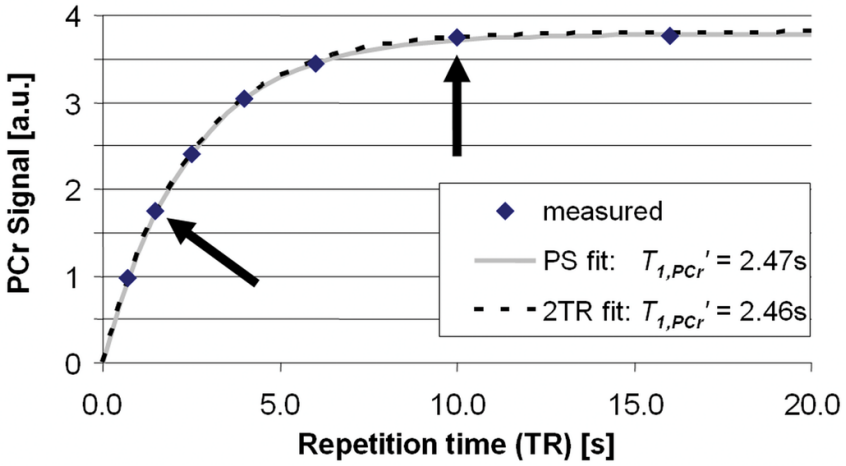

Figure 4.

Steady-state PCr signal (in arbitrary units, a.u.) measured as a function of TR (diamonds) while γ-ATP is saturated in one volunteer to determine $T_{1,PCr}'$. $T_{1,PCr}'$ was determined both by the conventional partial saturation by fitting all 7 data points (dotted line, relaxation curve), and by the 2TR method using only the data points acquired at TRs of 1.5s and 10s (arrows; the grey line is the corresponding implied relaxation curve).

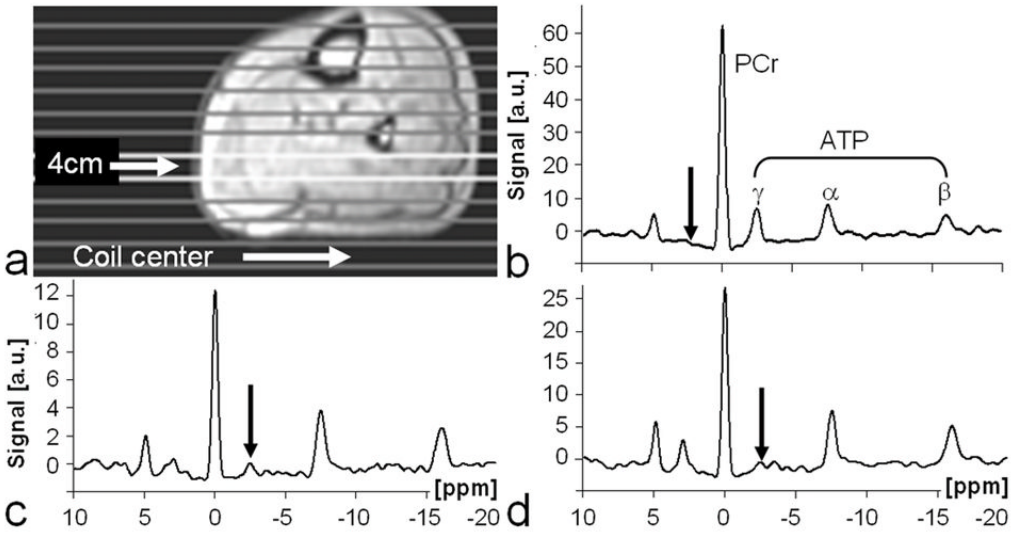

Figure 5.

Typical image and *TRiST* data from a human leg. (a) Axial ^{1}H image annotated with location of the coil center and 1D CSI slice positions. (b–d) ^{31}P spectra extracted from a slice at a depth of 4cm from the coil. The spectra were acquired with: (b) control saturation at a $TR_{control}$=25.0s to determine $M_{0,PCr}$; and with saturation of γ-ATP at (c) TR_{short}=1.5s and (d) TR_{long}=10.0s to determine $M_{0,PCr}'$ and $T_{1,PCr}'$. Note the different vertical scales (arbitrary units, a.u.). Arrows depict the location of the DANTE saturation.

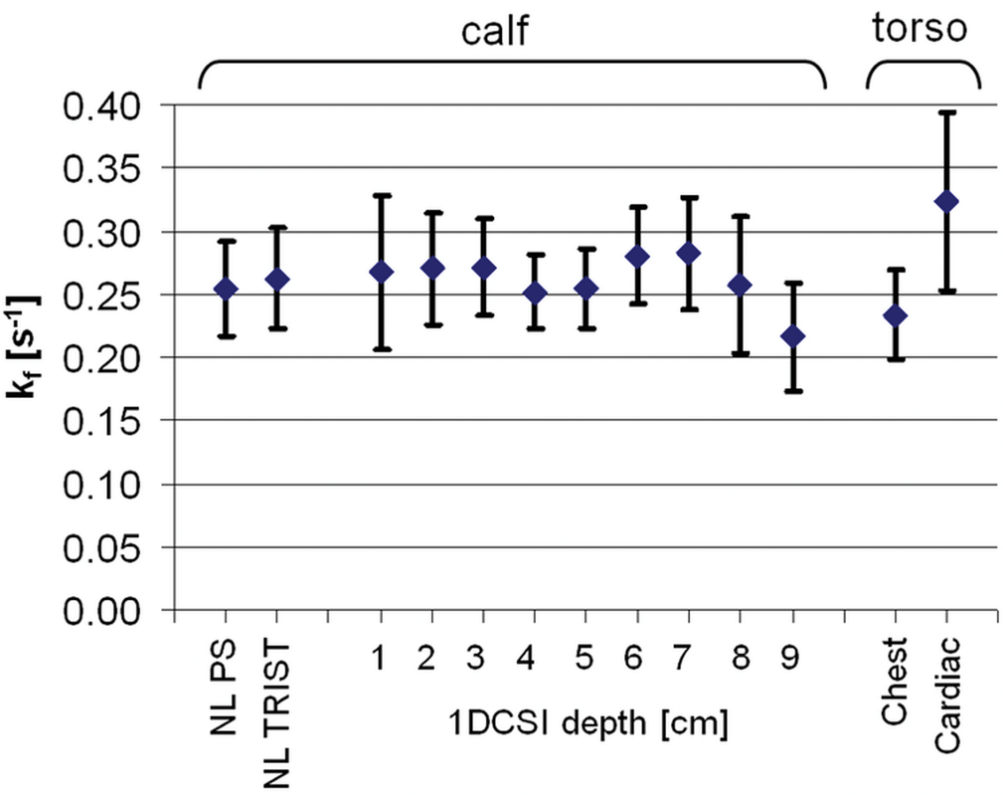

Figure 6.
Pseudo-first-order forward rate constants, k_f (means±SD) for the CK reaction measured *in-vivo* in the leg (n=6) and chest (n=8) at 3T. Values plotted from left to right are non-localized (NL) k_fs measured by conventional partial saturation (PS) and by *TRiST* in the calf muscle; k_fs measured by 1D CSI localized *TRiST* as a function of depth in the calf muscle; and k_fs measured in the chest and heart by *TRiST* 1D CSI, as indicated on the horizontal axis.

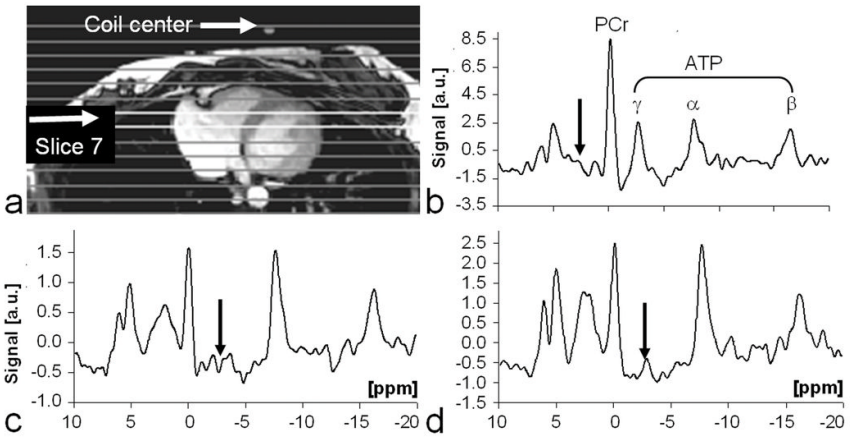

Figure 7.

Typical image and *TRiST* data from a human heart. (a) Axial ^{1}H image acquired at end-systole and annotated with the location of the coil center and 1D CSI slice positions. (b-d) Cardiac-gated ^{31}P heart spectra extracted from slice 7cm from the coil. The spectra were acquired with: (b) control saturation at a $TR_{control}$=16.1s to determine $M_{0,PCr}$; and with saturation of γ-ATP at (c) TR_{short}=1.7s, and at (d) TR_{long}=10.0s to determine $M_{0,PCr}'$ and $T_{1,PCr}'$. Note the different vertical scales (arbitrary units, a.u.). Arrows depict the location of the DANTE saturation.

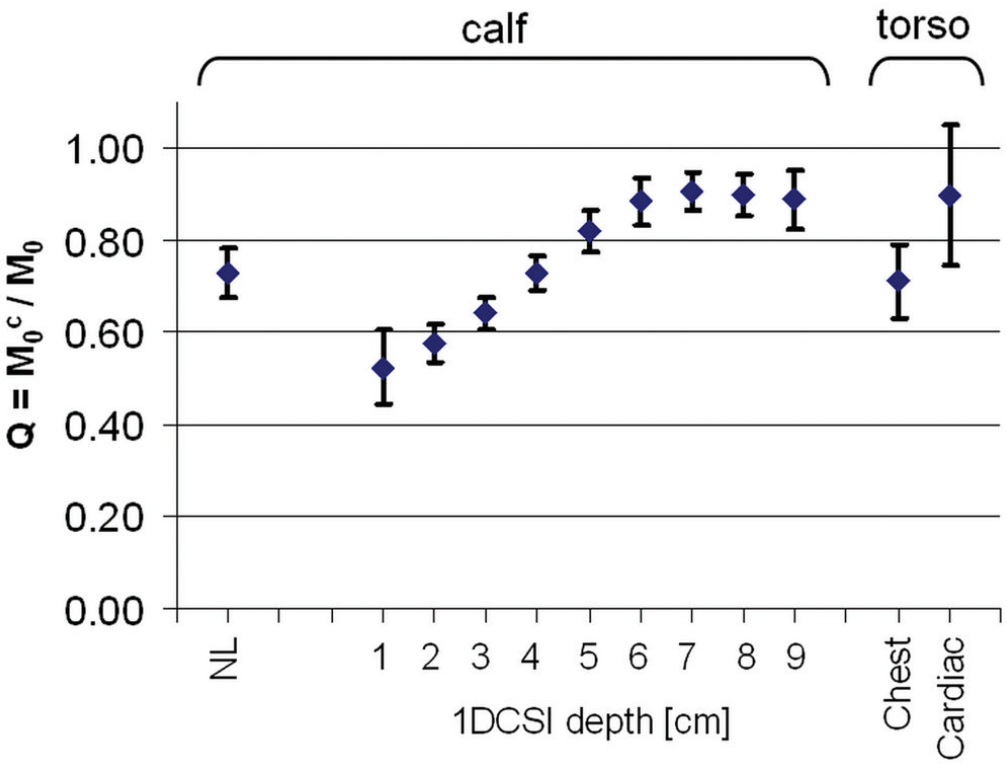

Figure 8.

Q (means±SD) measured *in-vivo* in human leg (n-6), chest, and heart (n=8). Values plotted from left to right are from non-localized (NL) studies of calf muscle; 1D CSI studies as a function of depth in the calf; and from 1D CSI studies of the chest and heart, as indicated on the horizontal axis. *Q* is a measure of spillover of the frequency selective saturation of the γ-ATP resonance onto the PCr resonance.

Table 1

The minimum flip angle β_{min} required to saturate $M_{z,\gamma\text{-}ATP}$ to below 5% of its equilibrium value over a bandwidth of 40Hz with the corresponding PCr spill-over Q for constant (m=1) and amplitude modulated (m=5) irradiation at 9cm depth and at the surface. Close to the coil, the flip-angle is about 6-times higher, increasing the spillover irradiation and reducing Q.

	m	β[°]	Q
β_{min} at 9cm depth	1	5.1	0.81
	5	0.9	0.93
at surface 6*β_{min}	1	30.6	0.11
	5	5.4	0.45